Journal of Data Analysis and Information Processing, 2021, 9, 30-50
https://www.scirp.org/journal/jdaip
ISSN Online: 2327-7203
ISSN Print: 2327-7211

Dynamic Deformation Monitoring of Lotsane Bridge Using Global Positioning Systems (GPS) and Linear Variable Differential Transducers (LVDT)

Selassie David Mayunga*, M. Bakaone

Department of Civil and Environmental Engineering, Botswana University of Science and Technology, Palapye, Botswana
Email: *mayungas@biust.ac.bw

How to cite this paper: Mayunga, S.D. and Bakaone, M. (2021) Dynamic Deformation Monitoring of Lotsane Bridge Using Global Positioning Systems (GPS) and Linear Variable Differential Transducers (LVDT). *Journal of Data Analysis and Information Processing*, **9**, 30-50.
https://doi.org/10.4236/jdaip.2021.91003

Received: August 12, 2020
Accepted: February 23, 2021
Published: February 26, 2021

Abstract

The measurements and analysis of deformation of engineering structures such as dams, bridges and high-rise buildings are important tasks for civil engineers. It is evident that, all civil engineering structures are susceptible for deterioration over a period of time. Bridges in particular, deteriorate due to loading conditions, environmental changes, earth movement, material used during construction, age and corrosion of steel. Continuous monitoring of such structure is the most important aspect as it provides quantitative information, assesses the state of the structure, detects unsafe positions and proposes early safety measures to be taken before it can threaten the safety of vehicles, goods and human life. Despite government's efforts to construct roads and highways, bridge deformation monitoring has not been given priority in most of African countries and ultimately causes some bridges to collapse unexpectedly. The purpose of this research is to integrate Global Positioning System (GPS) and Linear Variable Differential Transducers (LVDT) to monitor deformation of a bridge. The horizontal positions of reference and monitoring points were determined using Global Positioning System (GPS) while the vertical deflections, accelerations and strain were determined using Linear Variable Differential Transducers (LVDT). The maximum displacements obtained between zero and first epochs in x, y and z components were 0.798 m, at point LT08, 0.865 m at point BR13, and 0.56 m at point LT02 respectively. The maximum deflections for LVDT 1, 2 and 3 are 28.563 mm, 31.883 mm and 40.926 mm respectively. Finally, the correlation coefficient for the observations was 0.679 with standard deviations of 0.0168 and 0.0254 in x and y respectively. Our results identified some slight displacements in horizontal

components at the bridge.

Keywords

Bridge Deformation Monitoring, GPS and Linear Variable Differential Transducers

1. Introduction

Structural Health Monitoring (SHM) is a recent concept in civil engineering which aimed at assessing the behavior and safety of all civil engineering structures. The behavior and safety assessment include measurements and analysis of point positions on and away from the structure over different periods to determine the state of the structure. It is evident that all civil engineering structures such as bridges, high-rise buildings, dams, etc. are essential to social, human and economic development of any country. Bridges in particular, are key infrastructures to settlements, towns and cities which are susceptible for deterioration although are built to have life spans above three decades [1]. According to [2] deterioration is termed as a failure of a structure caused mainly by environmental and non-environmental factors such as erosion, earthquake, floods, loading conditions and construction materials which may have been overlooked during the design and construction periods. It is imperative to understand that, a bridge after being constructed it has to undergo static load test to verify the load deformation response. Therefore, continuous monitoring of bridges is an important aspect in obtaining information which helps to detect abnormal behavior of the structures at early stages and propose necessary safety measures before it can threaten the safety of vehicles, goods and human life. [3] pointed out that, continuous monitoring bridges are considered to be a valuable tool to complement other non-destructive methods in improving reliability and extending lifetime of the structure.

Bridge deformation monitoring is grouped into two major parts namely long term and short term [4]. Long term deformation monitoring is caused by a bridge foundation settlement, deck creep and stress relaxation, while short term deformation is caused by the dynamic effects such as wind, temperature, traffic, age and earthquake. Based on the measurements and analysis of data obtained, proper repair or rehabilitation can be conducted to keep the bridge safe and increase the life spans much longer. It is important to mention here that, the cost for monitoring and repair is much lower as compared to reconstruction cost of a new bridge. In recent years we have witnessed bridges collapsing in many parts in the world. In Italy for example, a bridge at Genoa collapsed killing dozens of people and damaged vehicles and other properties (https://www.euronews.com/tag/italya-daki-kopru-kazas-). In South Africa, a pedestrian bridge which was under construction collapsed along M1 highway

and damaged vehicles and properties. In the Southern District Council of Botswana, a bridge collapsed due to failed culvert which gave-in water pressure at a site of construction. According to a statement issued by the department of Roads, the bridge collapsed due to culvert failure causing loss of properties and resources of construction of a new bridge. Indeed, lack of short and long term bridge monitoring mechanism in most developing countries is a major factor for this phenomenon. Therefore, monitoring of bridges is very vital for safety of good, vehicles and the economic growth of any country. In order to effectively monitor the abnormal behavior of a bridge, a precise monitoring scheme is required. The standard practice for the monitoring of bridges in most developing countries has been periodical visual inspections, relying on inspectors to identify areas and signs of damages or unusual behaviors. Visual inspection is subjective in nature and does not provide reliable results [5] [6]. For decades, roads department at the Ministry of Works and Transport in Botswana has been collecting data on roads and bridge conditions. Data collected includes visual inspection of cracks, raveling, bleeding and rutting. However, visual inspection has serious shortcomings which include limited accuracy, subjective results, time consuming and cost ineffective. Based on visual inspection carried out in 2019, it shows that some of the bridges along A1 highway in the Central district have visible signs of damages. Apart from visual bridge inspections there have been no attempts made by the department to develop bridge monitoring mechanism. Lack of bridge monitoring mechanism may have been caused by limited resources, tools and advanced techniques.

Recent studies have attempted to utilize GPS for bridge deformation monitoring [7] [8]. [7] pointed out that GPS is capable of allowing redundant observations whereby the final precision of points can be determined using powerful least squares rigorous adjustment process. Apart from the advantages of GPS, there are limitations in its application. [9] used GPS to determine horizontal and vertical displacement of a bridge structure. In their study they showed that, GPS apart from measuring horizontal and vertical displacement it is also capable of determining frequency. There are various advantages of using GPS to monitor structural deformation including the determination of 3D displacements and its capability of being used in all weather conditions. In addition, data collected at each station is independent and is used in the adjustment process which can reach up to 10 - 20 Hz [10]. The obvious limitation is a lack of acquisition of redundant observation when used in real time kinematic [11] and pointed out that the most serious weakness of GPS is its lower accuracy in the determination of height, multipath error, cycle slips and slow sampling rate with real time Kinematic observation, the quality of the result is compromised by insufficient observations. [12] used GPS, Least Squares Solution and Kalman filter to determine horizontal and vertical displacements of a bridge. The result shows that, the displacements were obtained when the vehicle passes along the surface of the bridge and that the result obtained from

Kalman filter and Least Squares Solution were almost the same. [13] used GPS and a higher rate carrier receiver to monitor bridge deformation in a short baseline. The result shows that high rate receivers performed well which indicates that selection of best receiver can significantly improve the results. [14] used GPS, Wavelet Principal Component (WPC) analysis and Fast Fourier Transformation (FFT) to determine deformation effects of Monsoura Bridge in Egypt. The result shows that the Wavelet was effective in eliminating GPS noise encountered during GPS campaign. [15] used GPS in RTK mode and integrated with accelerometer sensor to determine dynamic displacement of Nottingham Bridge. In this study it was revealed that some errors from GPS and accelerometer were minimized by using double-differencing and the remaining errors were eliminated by multimode data acquisition technique from GPS. As stated above, however, general achievable accuracies with GPS in horizontal component are in the order of 1 cm. The accuracy is slightly bad in the height component which is mainly due to inherent geometric weakness and atmospheric errors which tend to increase when parts of the space is obstructed by other features and structures [16] [17]. In this work, we used GPS and LVDT for deformation monitoring of a bridge. Our objectives are to 1) determine dynamic displacement of Lotsane Bridge; 2) process and adjust the observations; 3) analyze the results and determine the dynamic behavior of the bridge; and 4) determine the displacements in the reference and monitoring points.

2. Materials and Methods

2.1 Study Area

Lotsane Bridge along Botswana A1 highway was selected as a case study for deformation monitoring. Lotsane Bridge is situated in Palapye 260 km north from Gaborone city, 168 km south of Francis town and 28 km from Serowe village. The bridge was constructed across Lotsane River and it is a link between Gaborone Capital city and neighboring city of Bulawayo in Zimbabwe. The bridge has 37.7 m long, 12 m wide and 9.6 m high. The bridge has two lanes in two way directions and was constructed using reinforcement concrete in three spans and supported with 3 pillars. **Figure 1** shows the design of Lotsane Bridge.

2.2. Planning and Establishment of Reference and Monitoring Points

The establishment of 8 reference and 14 monitoring points was done in 2019 which were located away and on the surface of the bridge respectively (Mayunga, S.D., and Thabo, 2019). The reference points were established and fixed on a stable ground while the monitoring points were fixed on the bridge with at equal intervals of 6 m at each sides of the bridge. Two baselines were used and their coordinates were determined using Sokkia GPS equipment. The GPS base was first set over BM5 control point and the rover measured both

reference and monitoring points for 20 minutes. The same process was repeated using a known point PMR33 to measure both reference and monitoring points. Figure 2 shows BM5 and PM33 and the configuration of reference and monitoring points.

2.3. Measuring the Stress of the Bridge

Three LVDT sensors were placed midway of the bridge where the maximum deflection was likely to occur and had room to displace up and down without any constraint. To minimize the observation errors, the LVDTs locations were in constant contact with the steel members of the bridge. One data set consisted of three linear displacement readings were measured in millimeters (mm) and an acceleration data were measured in (g). The observations were repeated throughout the day to obtain sufficient amount of data and saved as a time-series graph and numerical data.

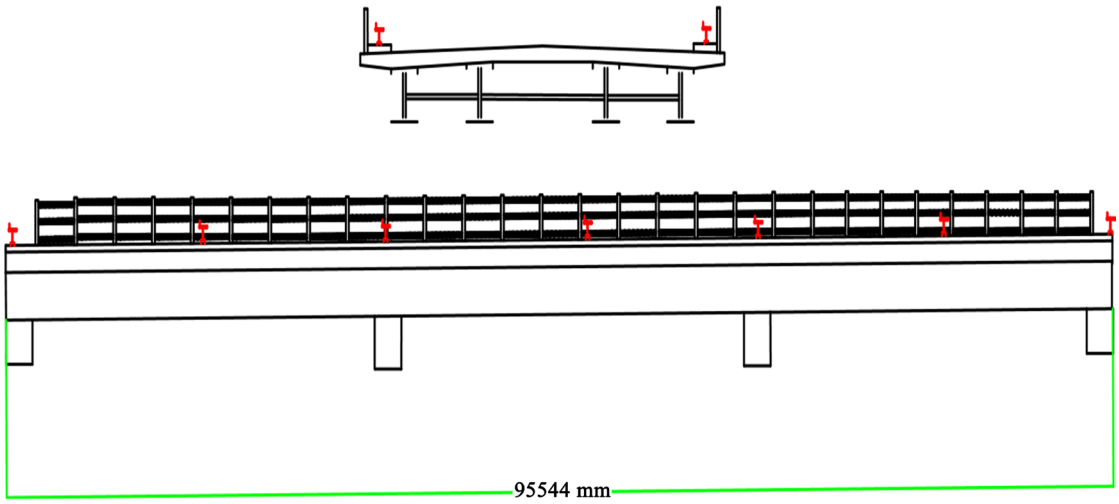

Figure 1. Design of Lotsane bridge, Palapye, Botswana.

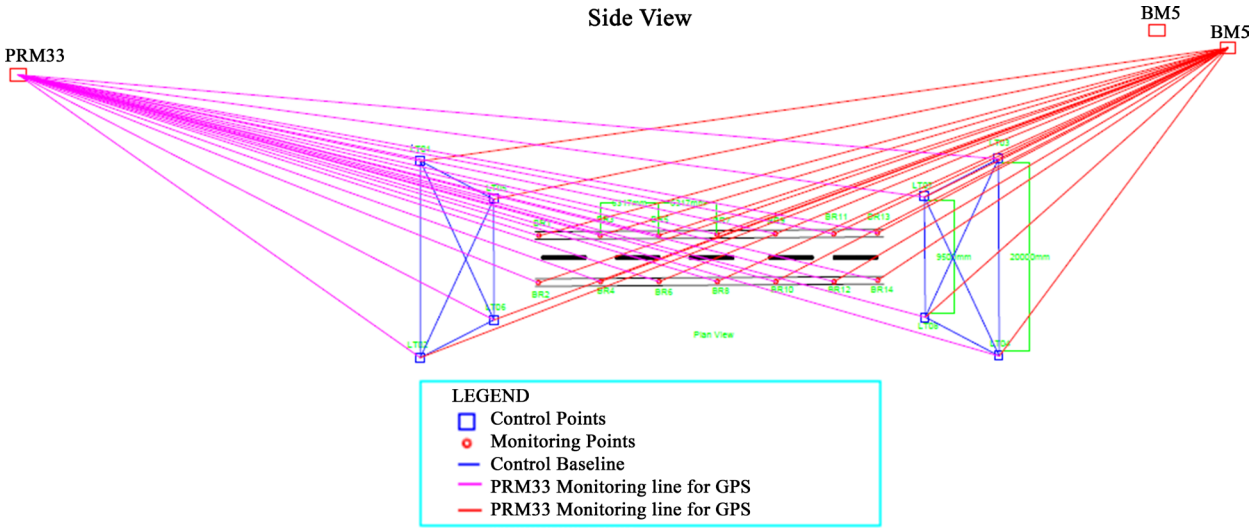

Figure 2. Observation of reference and monitoring points.

2.4. GPS Data Processing

After GPS observations of reference and monitoring points at first epoch, raw data were stored into the internal memory of the receiver and downloaded into the computer derived and adjusted by least squares adjustment using Magnet processing software to determine the reliability of the adjusted coordinates. The GPS reference and monitoring points were adjusted using Least Squares Solution using the following mathematical relationship:

Let line *ij* be from point (*i*) to (*j*) the observation equation is written as:

$$X_j = X_i + \Delta X_{ij} + vx_{ij} \tag{1}$$

$$Y_j = Y_i + \Delta Y_{ij} + vy_{ij} \tag{2}$$

$$Z_j = Z_i + \Delta Z_{ij} + vz_{ij} \tag{3}$$

Equations (1)-(3) can be compressed in matrix format as:

$$\begin{pmatrix} x_1 \\ x_2 \\ x_3 \\ \vdots \\ x_n \end{pmatrix} = \begin{pmatrix} l_1 \\ l_2 \\ l_3 \\ \vdots \\ l_n \end{pmatrix} + \begin{pmatrix} v_1 \\ v_2 \\ v_3 \\ \vdots \\ v_n \end{pmatrix} \tag{4}$$

$$AX = L + V \tag{5}$$

where:

A is the design matrix;

X is the vector of unknowns;

L is the vector of observations and;

V is the vector of residuals.

By inserting a weight (w) and a priori variance σ_o^2 for the observations in Equation (4), the cofactor matrix can be given as:

$$Q_L = \frac{1}{\sigma_o^2} Sum_L \tag{6}$$

Therefore,

$$W = Q_L^{-1} \tag{7}$$

The solution becomes well defined by Least Squares principle of $V^{\mathrm{T}}WV$ = minimum. From the above observation equations the least squares principle becomes:

$$\left(A^{\mathrm{T}}WA\right)X = A^{\mathrm{T}}WL \tag{8}$$

The vector of unknown can be computed as:

$$X = \left(A^{\mathrm{T}}WA\right)^{-1}\left(A^{\mathrm{T}}WL\right) \tag{9}$$

The matrix equation can be computed as:

$$V = AX - L \tag{10}$$

The standard deviation of the measurements of unit weight for the weighted

observations is given as:

$$\sigma_0 = \sqrt{\frac{V^{\mathrm{T}}WV}{r}} \tag{11}$$

where, r is the degree of freedom in the adjustment which is equal to the number of observations minus the number of unknowns.

2.5. LVDT Data Processing

The highly precise, universal, and reliable data acquisition system QuantumX was combined with WA-T HBM's sensors and the Catman software to have a complete measurement and testing solution. Catman software was used for data acquisition and analysis of the observations. From the sensor to the software, simply "plug and measure" principle was used to determine the displacement results for each sensor.

3. Results

3.1. Results from GPS Observations

The final coordinates of reference and monitoring points for zero epoch results were obtained after adjusted using Least Squares principle. Table 1 and Table 2 below show the final coordinates of zero and first epochs which will be used to determine deformation between zero and first epochs. Figure 3, Figure 4 and Figure 5 show the horizontal displacement of some control points like LT5, LT6, LT7 and LT8 which behave as outliers based on their graph trends. The errors on those control points might have been caused by the contractions and expansions characteristics of the soil since there have been some heavy rains between zero and first epochs. Also the discrepancies on the X and Y directions could have been caused erosion of the river soils and vibrations of the bridge due to living loadings. Figure 6 displays the pattern of displacement in the Z-axis on which LT4, LT5, LT6 and LT7 were highly affected. These control points are on vicinity where there is movement so it might be assumed that humans or animals tempered with them, hence resulted in their vertical displacements. Figure 7 shows coordinate differences in x, y and z for zero and first epochs while Figure 8 shows the differences of LVDT 1, 3 and 2 respectively. Figures 9-11 shows frequency charts for LVDT 1, 3, and 2 respectively.

3.2. The Correlation Coefficient

The correlation coefficient for the observations, denoted by ρ, tells how closely data in a scatterplot fall along a straight line. The closer that the absolute value of ρ is close to one, the better that the data are described by a linear equation. If $\hat{\rho} = 1$ or $\hat{\rho} = -1$ then the data set is perfectly aligned. Data sets with values of ρ close to zero show little to no straight-line relationship.

$$\hat{\rho} = \frac{S_{xy}}{S_x S_y} \tag{15}$$

Table 1. Final adjusted GPS coordinates obtained from zero epoch (2019).

Name	Northing (m)	Easting (m)	Heights (m)
LT01	2,494,370.393	−8565.250	919.341
LT02	2,494,343.838	−8515.565	918.928
LT03	2,494,332.774	−8579.381	918.478
LT04	2,494,312.603	−8553.984	918.238
LT05	2,494,224.355	−8678.514	919.688
LT06	2,494,188.693	−8636.932	919.631
LT07	2,494,245.301	−8658.604	918.489
LT08	2,494,226.059	−8622.229	918.748
BR01	2,494,285.520	−8590.892	920.522
BR02	2,494,290.460	−8597.178	920.521
BR03	2,494,280.551	−8594.739	920.562
BR04	2,494,285.511	−8601.071	920.581
BR05	2,494,275.613	−8598.553	920.575
BR06	2,494,280.582	−8604.914	920.586
BR07	2,494,270.652	−8602.370	920.590
BR08	2,494,275.593	−8608.755	920.604
BR09	2,494,265.742	−8606.255	920.590
BR10	2,494,270.688	−8612.587	920.595
BR11	2,494,260.811	−8610.097	920.567
BR12	2,494,265.691	−8616.379	920.570
BR13	2,494,255.817	−8613.918	920.510
BR14	2,494,260.823	−8620.304	920.527

Table 2. Final adjusted GPS coordinates computed from first epoch (2020).

Name	Northing (m)	Easting (m)	Heights (m)
LT01	2,494,370.454	−8565.396	919.341
LT02	2,494,332.824	−8515.532	918.928
LT03	2,494,332.774	−8579.746	918.478
LT04	2,494,312.603	−8553.984	918.238
LT05	2,494,224.355	−8678.673	919.688
LT06	2,494,188.693	−8637.081	919.631
LT07	2,494,245.301	−8554.141	918.489
LT08	2,494,226.059	−8515.693	918.748
BR01	2,494,285.583	−8590.892	920.522
BR02	2,494,290.496	−8597.178	920.521
BR03	2,494,280.609	−8594.739	920.562

Continued

BR04	2,494,285.553	−8601.071	920.581
BR05	2,494,275.692	−8598.553	920.575
BR06	2,494,280.624	−8604.914	920.586
BR07	2,494,270.734	−8602.370	920.590
BR08	2,494,275.666	−8608.755	920.604
BR09	2,494,265.814	−8606.255	920.590
BR10	2,494,270.758	−8612.587	920.595
BR11	2,494,260.876	−8610.097	920.567
BR12	2,494,265.748	−8616.379	920.570
BR13	2,494,255.888	−8613.918	920.510
BR14	2,494,260.874	−8620.304	920.527

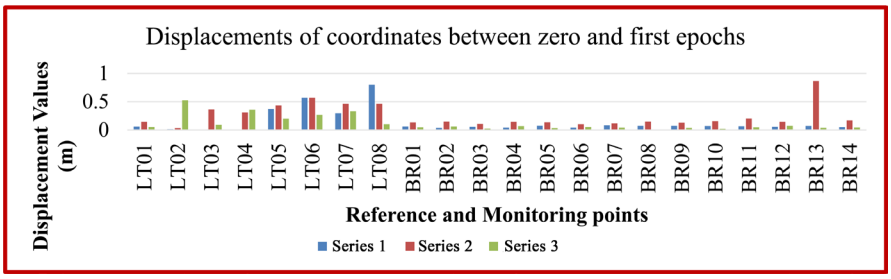

Figure 3. Coordinate difference from zero epoch in Δx, Δy *and* Δz.

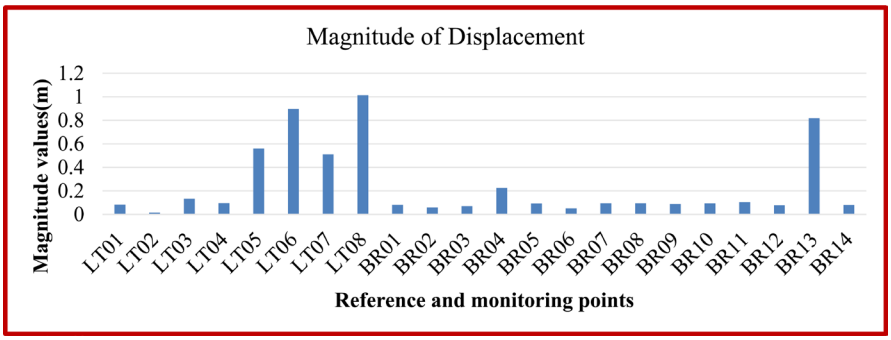

Figure 4. Magnitude of displacement of reference and monitoring points between zero and first epoch.

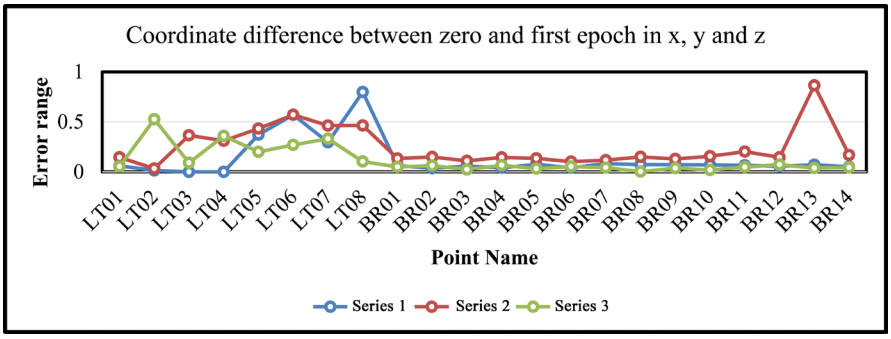

Figure 5. Displacement pattern in Δx, Δy *and* Δz between zero and first epochs.

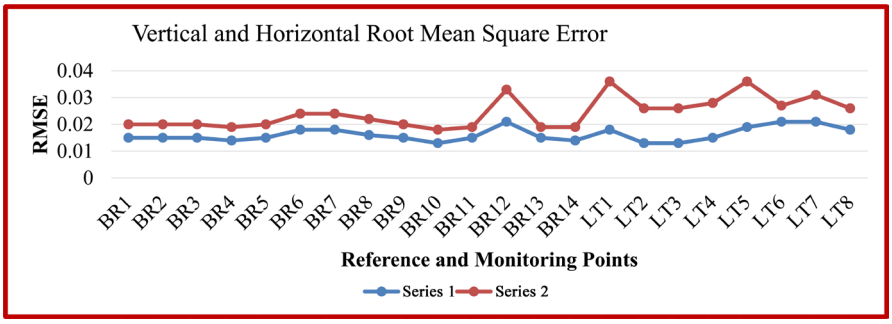

Figure 6. Residuals of reference and monitoring points from GPS observation between zero and first epochs.

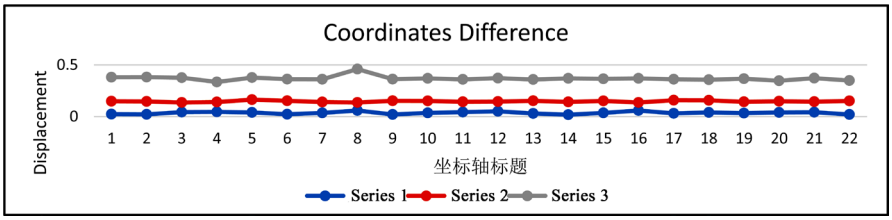

Figure 7. Coordinates differences in *x*, *y* and *z*.

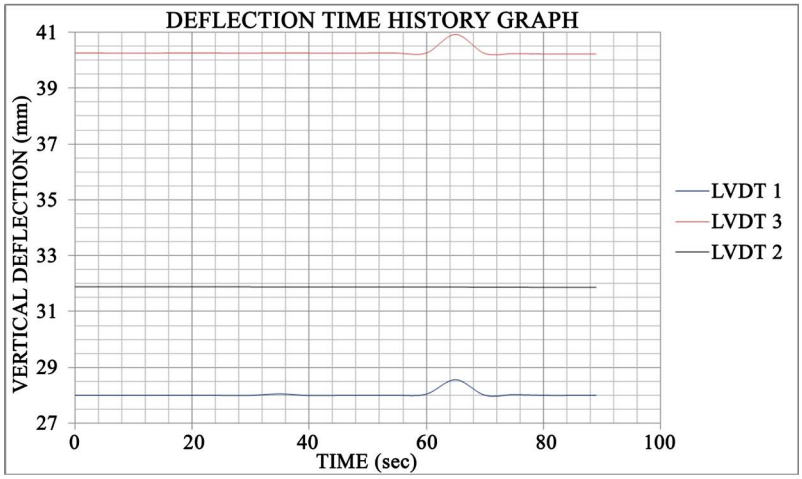

Figure 8. Deflection of LVDT 1, 2 and 3.

where:

$$\bar{x} = 0.016227$$

$$\bar{y} = 0.024227$$

$$s_{xy} = \sum \frac{(x-\bar{x})(y-\bar{y})}{n-1} \tag{16}$$

$$s_{xy} = \frac{0.000209864}{21} = 9.993\times10^{-6}$$

$$s_x^2 = \sum \frac{(x-\bar{x})^2}{n-1} \tag{17}$$

$$s_x^2 = \frac{0.000141864}{21} = 6.755\times10^{-6}$$

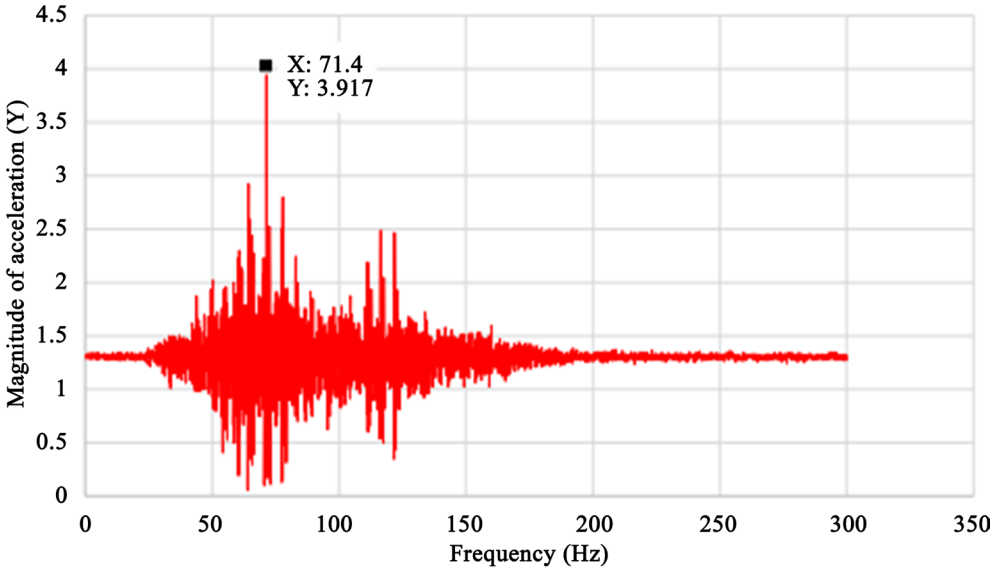

Figure 9. Frequency chart for LVDT 1.

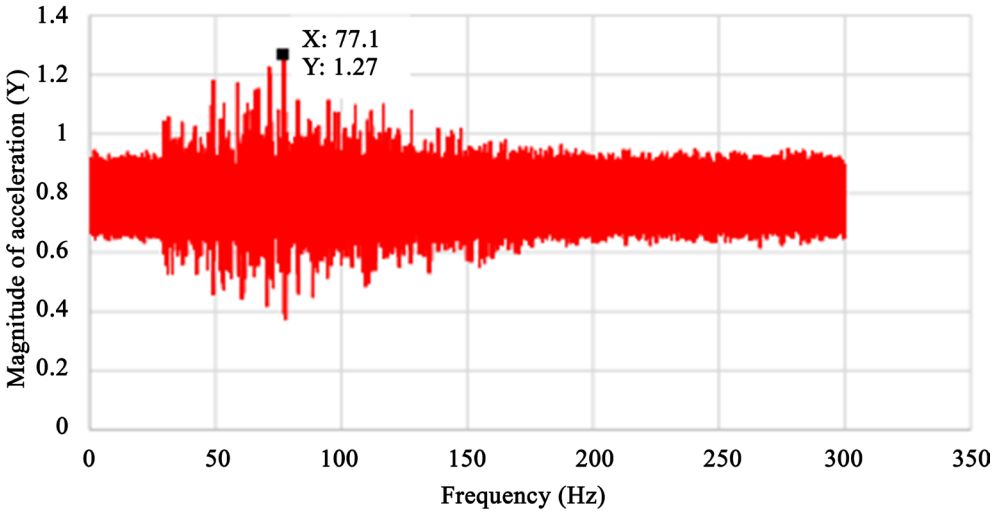

Figure 10. Frequency chart for LVDT 2.

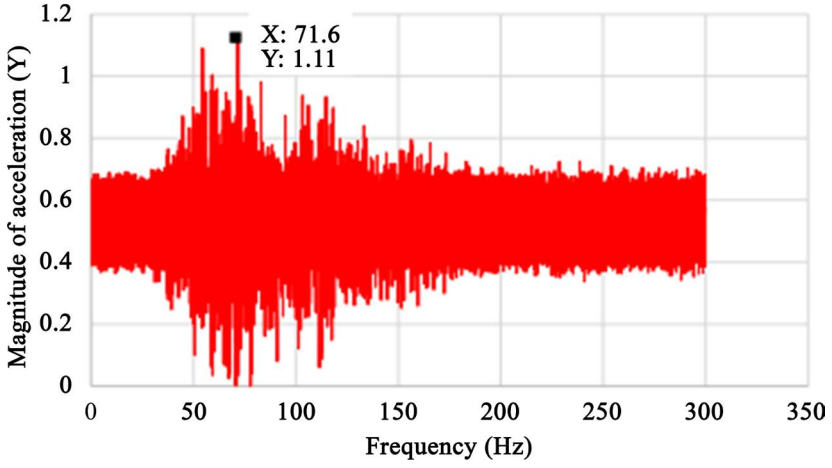

Figure 11. Frequency chart for LVDT 3.

$$s_y^2 = \sum \frac{(y-\bar{y})^2}{n-1} \tag{18}$$

$$s_y^2 = \frac{0.000673864}{21} = 3.20887\times10^{-5}$$

$$\hat{\rho} = \frac{9.99351\times10^{-6}}{0.002599117\times0.00566493} = 0.679$$

The Standard Deviations

$$\sigma_x = \sqrt{\frac{\sum_{n=1}^{n} v_x^2}{n-1}} \tag{19}$$

$$\sigma_x = 0.0168$$

$$\sigma_y = \sqrt{\frac{\sum_{n=1}^{n} v_y^2}{n-1}} \tag{20}$$

$$\sigma_y = 0.0254$$

where:

σ_x = Standard deviation;

n = sample;

v = residuals.

4. Discussion

4.1 GPS Data Analysis

The GPS observations and adjustment of reference and monitoring points of zero epochs were processed in 2019 while GPS observations and adjustment of reference and monitoring points of first epoch were processed in 2020. The final adjusted GPS coordinates for zero and first epochs were computed and compared to determine whether there are displacements within the epochs. Table 3 shows the comparison of coordinates between zero and first epoch while Table 4 shows the difference in coordinates in x, y and z between epochs. The outliers might have been caused by movements of reference points due to heavy rains experienced in 2020. The maximum residuals between zero and first epoch are 0.021 m and 0.036 m in x and y respectively, which all fall on the possible magnitudes for systematic GPS errors. All directions of displacement for reference and monitoring points are in the first quadrant as shown in Table 5. Table 6, Table 7, Tables 10-12 show the residuals of observations in x and y, magnitude of displacement, final coordinates of reference and monitoring points, deflection values of LVDT respectively.

4.2. Results from LVDT Observations

Table 8 below shows the data obtained using a series of three LVDT's to determine the vertical deflections from traffic loadings on the Lotsane Bridge.

The output signal of the frequency domain is shown by Figures 9-11. From the figures, the peak frequencies formed are an estimate of the natural frequency of the bridge section and it clearly shows the dominant frequency of 77.1 Hz on LVDT 2.

Table 3. Comparison of GPS coordinates between zero (2019) and first epoch (2020).

Name	Northing (m) Zero Epoch	Easting (m) Zero Epoch	Heights (m) Zero Epoch	Northing (m) First Epoch	Easting (m) First Epoch	Heights (m) First Epoch
LT01	2,494,370.393	−8565.250	919.341	2,494,370.454	−8565.396	919.288
LT02	2,494,343.838	−8515.565	918.928	2,494,343.824	8515.532	918.402
LT03	2,494,332.774	−8579.381	918.478	2,494,332.774	−8579.746	918.387
LT04	2,494,312.603	−8553.984	918.238	2,494,312.603	−8678.673	918.597
LT05	2,494,224.355	−8678.514	919.688	2,494,224.727	−8678.081	919.488
LT06	2,494,188.693	−8636.932	919.631	2,494,188.122	−8636.361	919.361
LT07	2,494,245.301	−8658.604	918.489	2,494,245.597	−8658.141	918.158
LT08	2,494,226.059	−8622.229	918.748	2,494,226.857	−8622.693	918.852
BR01	2,494,285.520	−8590.892	920.522	2,494,285.583	−8590.026	920.473
BR02	2,494,290.460	−8597.178	920.521	2,494,290.496	−8597.327	920.458
BR03	2,494,280.551	−8594.739	920.562	2,494,280.609	−8594.849	920.538
BR04	2,494,285.511	−8601.071	920.581	2,494,285.553	−8601.216	920.514
BR05	2,494,275.613	−8598.553	920.575	2,494,275.692	−8598.688	920.543
BR06	2,494,280.582	−8604.914	920.586	2,494,280.624	−8605.017	920.532
BR07	2,494,270.652	−8602.370	920.590	2,494,270.734	−8602.487	920.548
BR08	2,494,275.593	−8608.755	920.604	2,494,275.666	−8608.905	920.574
BR09	2,494,265.742	−8606.255	920.590	2,494,265.814	−8606.384	920.553
BR10	2,494,270.688	−8612.587	920.595	2,494,270.758	−8612.743	920.576
BR11	2,494,260.811	−8610.097	920.567	2,494,260.876	−8610.299	920.519
BR12	2,494,265.691	−8616.379	920.570	2,494,265.748	−8616.525	920.497
BR13	2,494,255.817	−8613.918	920.510	2,494,255.888	−8614.053	920.471
BR14	2,494,260.823	−8620.304	920.527	2,494,260.874	−8620.472	920.483

Table 4. Adjusted GPS coordinates between zero (2019) and first epochs (2020) in ΔN, ΔE, and ΔH.

Name	ΔN (m) Zero Epoch to First Epoch	ΔE (m) Zero Epoch to First Epoch	ΔH (m) Zero Epoch to First Epoch
LT01	0.061	0.146	0.053
LT02	0.014	0.033	0.526
LT03	0.000	0.365	0.091
LT04	0.000	0.311	0.359
LT05	0.372	0.433	0.200
LT06	0.571	0.571	0.270
LT07	0.296	0.463	0.331
LT08	0.798	0.464	0.104
BR01	0.063	0.134	0.049
BR02	0.036	0.149	0.063
BR03	0.058	0.110	0.024
BR04	0.042	0.145	0.067

Continued

BR05	0.075	0.135	0.032
BR06	0.042	0.103	0.054
BR07	0.082	0.117	0.042
BR08	0.073	0.150	0.003
BR09	0.072	0.129	0.037
BR10	0.070	0.156	0.019
BR11	0.065	0.202	0.048
BR12	0.057	0.146	0.073
BR13	0.071	0.865	0.039
BR14	0.051	0.168	0.044

Table 5. Shows the horizontal and vertical magnitude displacement and direction of displacements.

Name	ΔE (m) Zero Epoch to First Epoch	ΔN (m) Zero Epoch to First Epoch	ΔZ (m) Zero Epoch to First Epoch	Magnitude of displacement D_a (m)	Direction of displacement θ
LT01	0.061	0.146	0.053	0.082	67˚19'28"
LT02	0.014	0.033	0.526	0.015	67˚00'40"
LT03	0.000	0.365	0.091	0.133	00˚00'00"
LT04	0.000	0.311	0.359	0.096	00˚00'00"
LT05	0.372	0.433	0.200	0.559	49˚20'00"
LT06	0.571	0.571	0.270	0.897	45˚00'00"
LT07	0.296	0.463	0.331	0.510	57˚24'32"
LT08	0.798	0.464	0.104	1.013	30˚10'34"
BR01	0.063	0.134	0.049	0.080	64˚49'10"
BR02	0.036	0.149	0.063	0.058	76˚25'01"
BR03	0.058	0.110	0.024	0.070	62˚11'54"
BR04	0.042	0.145	0.067	0.225	73˚50'45"
BR05	0.075	0.135	0.032	0.093	60˚56'43"
BR06	0.042	0.103	0.054	0.052	67˚48'57"
BR07	0.082	0.117	0.042	0.095	54˚58'30"
BR08	0.073	0.150	0.003	0.095	64˚02'57"
BR09	0.072	0.129	0.037	0.088	60˚49'56"
BR10	0.070	0.156	0.019	0.094	65˚50'00"
BR11	0.065	0.202	0.048	0.105	72˚09'45"
BR12	0.057	0.146	0.073	0.078	68˚40'25"
BR13	0.071	0.865	0.039	0.819	85˚18'27"
BR14	0.051	0.168	0.044	0.079	73˚06'47"

Table 6. Residuals of reference and monitoring points from GPS observation.

Point No.	Residual in x	Residual in y
BR1	0.015	0.020
BR2	0.015	0.020
BR3	0.015	0.020
BR4	0.014	0.019
BR5	0.015	0.020
BR6	0.018	0.024
BR7	0.018	0.024
BR8	0.016	0.022
BR9	0.015	0.020
BR10	0.013	0.018
BR11	0.015	0.019
BR12	0.021	0.033
BR13	0.015	0.019
BR14	0.014	0.019
LT1	0.018	0.036
LT2	0.013	0.026
LT3	0.013	0.026
LT4	0.015	0.028
LT5	0.019	0.036
LT6	0.021	0.027
LT7	0.021	0.031
LT8	0.018	0.026

Table 7. Magnitude of displacement in *x*, *y* and *z*.

Name	*dN* (m)	*dE* (m)	*dHt* (m)	Horz RMS	Vert RMS
PRM33–PRM30	−367.537	−158.898	1.108	0.002	0.003
PRM33–LT-01	1110.753	565.95	−4.814	0.002	0.003
PRM33–LT-02	1084.198	615.635	−5.225	0.002	0.003
PRM33–LT-03	1073.134	551.819	−5.675	0.002	0.003
PRM33–LT-04	1052.963	577.216	−5.91	0.002	0.003
PRM33–LT-05	964.715	452.686	−4.482	0.002	0.003
PRM33–LT-06	929.053	494.268	−4.627	0.002	0.003
PRM33–LT-07	985.661	472.596	−5.67	0.002	0.003
PRM33–LT-08	966.419	508.971	−5.688	0.002	0.003
PRM33–BR-01	1025.88	540.308	−3.637	0.002	0.003
PRM33–BR-02	1030.82	534.022	−3.628	0.002	0.003

Continued

PRM33–BR-03	1020.911	536.461	−3.592	0.002	0.003
PRM33–BR-04	1025.871	530.129	−3.582	0.002	0.003
PRM33–BR-05	1015.973	532.647	−3.576	0.002	0.004
PRM33–BR-06	1020.942	526.286	−3.559	0.002	0.003
PRM33–BR-07	1011.012	528.83	−3.573	0.002	0.003
PRM33–BR-08	1015.953	522.445	−3.538	0.002	0.003
PRM33–BR-09	1006.102	524.945	−3.573	0.002	0.003
PRM33–BR-10	1011.048	518.613	−3.554	0.002	0.003
PRM33–BR-11	1001.171	521.103	−3.601	0.002	0.003
PRM33–BR-12	1006.051	514.821	−3.577	0.002	0.003
PRM33–BR-13	996.177	517.282	−3.651	0.002	0.003
PRM33–BR-14	1001.183	510.896	−3.623	0.002	0.003

Table 8. Comparison of GPS height and precise leveling.

	Reference point = PRM33			Reference Point = BM5			Coordinate Differences		
	2,493,259.640	−9131.200	930.26	2,499,267.47	−13,034.15	982.77			
Name	Northing (m)	Easting (m)	*H*	Northing (m)	Easting (m)	*Ht*	ΔNorthings (m)	ΔEastings (m)	Δ*H* (m)
LT01	2,494,370.393	−8565.25	925.255	2,494,370.416	−8565.398	925.635	0.023	0.148	0.380
LT02	2,494,343.838	−8515.565	924.843	2,494,343.859	−8515.711	925.224	0.021	0.146	0.381
LT03	2,494,332.774	−8579.381	924.394	2,494,332.817	−8579.517	924.77	0.043	0.136	0.376
LT04	2,494,312.603	−8553.984	924.158	2,494,312.558	−8554.124	924.492	0.045	0.140	0.334
LT05	2,494,224.355	−8678.514	925.587	2,494,224.395	−8678.677	925.964	0.04	0.163	0.377
LT06	2,494,188.693	−8636.932	925.442	2,494,188.715	−8637.084	925.804	0.022	0.152	0.362
LT07	2,494,245.301	−8658.604	924.399	2,494,245.336	−8658.744	924.759	0.035	0.140	0.360
LT08	2,494,226.059	−8622.229	924.38	2,494,226.117	−8622.365	924.839	0.058	0.136	0.459
BR01	2,494,285.520	−8590.892	926.432	2,494,285.540	−8591.044	926.794	0.02	0.152	0.362
BR02	2,494,290.460	−8597.178	926.441	2,494,290.495	−8597.329	926.81	0.035	0.151	0.369
BR03	2,494,280.551	−8594.739	926.477	2,494,280.594	−8594.882	926.836	0.043	0.143	0.359
BR04	2,494,285.511	−8601.071	926.487	2,494,285.561	−8601.216	926.859	0.05	0.145	0.372
BR05	2,494,275.613	−8598.553	926.493	2,494,275.643	−8598.705	926.851	0.03	0.152	0.358
BR06	2,494,280.582	−8604.914	926.51	2,494,280.600	−8605.055	926.879	0.018	0.141	0.369
BR07	2,494,270.652	−8602.37	926.495	2,494,270.687	−8602.521	926.86	0.035	0.151	0.365
BR08	2,494,275.593	−8608.755	926.531	2,494,275.651	−8608.891	926.9	0.058	0.136	0.369
BR09	2,494,265.742	−8606.255	926.496	2,494,265.773	−8606.413	926.857	0.031	0.158	0.361
BR10	2,494,270.688	−8612.587	926.515	2,494,270.728	−8612.744	926.871	0.04	0.157	0.356
BR11	2,494,260.811	−8610.097	926.468	2,494,260.844	−8610.24	926.834	0.033	0.143	0.366
BR12	2,494,265.691	−8616.379	926.492	2,494,265.731	−8616.527	926.838	0.04	0.148	0.346
BR13	2,494,255.817	−8613.918	926.418	2,494,255.859	−8614.062	926.79	0.042	0.144	0.372
BR14	2,494,260.823	−8620.304	926.446	2,494,260.843	−8620.455	926.795	0.02	0.151	0.349

Table 9. Comparison of GPS height and precise leveling.

Point	GPS height (m)	Precise Levelling (m)	Difference ($\Delta H_{GPS} - \Delta H_{LEVEL}$) (m)
LT01	925.255	919.341	5.914
LT02	924.843	918.928	5.915
LT03	924.394	918.478	5.916
LT04	924.158	918.238	5.920
LT05	925.587	919.688	5.899
LT06	925.442	919.631	5.811
LT08	924.399	918.489	8.910
BR01	924.380	918.748	5.632
BR02	926.432	920.522	5.910
BR03	926.477	920.562	5.917
BR04	926.487	920.581	9.906
BR05	926.493	920.575	5.924
BR06	926.510	920.586	5.924
BR07	926.531	920.590	5.905
BR08	926.531	920.590	5.927
BR09	926.496	920.590	5.906
BR10	926.515	920.595	5.920
BR11	926.468	920.567	5.901
BR12	926.492	920.570	5.922
BR13	926.418	920.510	5.908
BR14	926.446	920.527	5.919

Table 10. Final coordinates of reference and monitoring points.

Name	Northing (m)	Easting (m)	Heights (m)
LT01	2,494,370.393	−8565.25	919.341
LT02	2,494,343.838	−8515.565	918.928
LT03	2,494,332.774	−8579.381	918.478
LT04	2,494,312.603	−8553.984	918.238
LT05	2,494,224.355	−8678.514	919.688
LT06	2,494,188.693	−8636.932	919.631
LT07	2,494,245.301	−8658.604	918.489
LT08	2,494,226.059	−8622.229	918.748
BR01	2,494,285.520	−8590.892	920.522
BR02	2,494,290.460	−8597.178	920.521
BR03	2,494,280.551	−8594.739	920.562
BR04	2,494,285.511	−8601.071	920.581

Continued

BR05	2,494,275.613	−8598.553	920.575
BR06	2,494,280.582	−8604.914	920.586
BR07	2,494,270.652	−8602.370	920.590
BR08	2,494,275.593	−8608.755	920.604
BR09	2,494,265.742	−8606.255	920.590
BR10	2,494,270.688	−8612.587	920.595
BR11	2,494,260.811	−8610.097	920.567
BR12	2,494,265.691	−8616.379	920.570
BR13	2,494,255.817	−8613.918	920.510
BR14	2,494,260.823	−8620.304	920.527

Table 11. Field deflection-time data for LVDT.

TIME (sec)	VERTICAL DEFLECTION (mm)		
	LVDT 1	LVDT 3	LVDT 2
0	28.00647	40.25415	31.89259
5	28.00443	40.25446	31.89188
10	28.00263	40.25342	31.89075
15	28.00351	40.25442	31.88909
20	28.0007	40.25384	31.88822
25	27.99938	40.25355	31.88642
30	28.00009	40.25264	31.88548
35	28.05152	40.25834	31.88361
40	27.99379	40.25397	31.88337
45	28.00124	40.25169	31.88234
50	28.00156	40.25399	31.8814
55	28.0027	40.25428	31.87992
60	28.04368	40.25927	31.87911
65	28.56282	40.92585	31.88283
70	28.00369	40.24071	31.87436
75	28.02768	40.2412	31.87367
80	28.00042	40.22477	31.87115
85	27.99855	40.22374	31.86828
89	27.99936	40.22451	31.86819

Table 12. Deflection of the bridge from LVDT.

Span	Position 1	Position 2	Position 3
LVDT	LVDT 1	LVDT2	LVDT3
Maximum Deflection (mm)	28.56282	31.88283	40.92585

4.3. Live-Load Deflections

According to AASHTO Standard Specifications (AASHTO, 1996), the limits live-load deflections is $L/800$ for ordinary bridges and $L/1000$ for bridges in urban areas that are subject to pedestrian use. Therefore, for Lotsane Bridge the maximum limit is expressed as shown in Equation (21).

$$\frac{L}{800} \tag{21}$$

where L is the length of the bridge in m.

Therefore the maximum deflection is given as $\frac{37.7\text{ m}}{800} = 47.125\text{ mm}$.

4.4. Analysis of LVDT Results

The deflection produced by moving traffic loads on the surface of the bridge shows that the maximum deflection observed was 40.925 mm. The AASHTO Standard Specification (AASHTO, 1996) limits live-load deflections to $L/800$ for ordinary bridges and $L/1000$ for bridges in urban areas that are subject to pedestrian use. These limits are required for steel, pre-stressed and reinforced concrete, and other bridge superstructure types. The computed limit live-load deflection for Lotsane Bridge was 47.125 mm. Therefore the bridge's performance with regards to deflections is within the tolerable limit. Finally, the natural filter frequency of the bridge was found to be 50 Hz in the vertical direction using Bessel low pass filter characteristics.

5. Conclusions

Based on this study, the analysis of results rests on the following conclusions:

1) The proposed integrated deformation monitoring scheme using GPS and RTK can provide valuable deformation data of the bridge structure.

2) It was revealed that the maximum displacements detected between zero and first epochs in x, y and z components are 0.798 m, at point LT08, 0.865 m at point BR13, and 0.56 m at point LT02 respectively. 3. The traffic loads are the main factor affecting bridge cracks.

4) The maximum displacements for sensors 1, 2 and 3 are 28.563 mm, 31.883 mm and 40.926 mm respectively.

5) The computed maximum live-load deflection for Lotsane Bridge was 47.125 mm against 4.09 mm obtained by LVDT which indicates that the bridge's performance is within the recommended limit.

6) The correlation coefficient for the observations was 0.679 with standard deviations of 0.0168 and 0.0254 in x and y respectively.

Acknowledgements

This work was supported by Botswana International University of Science and Technology.

Conflicts of Interest

The authors declare no conflicts of interest regarding the publication of this paper.

References

[1] Beshr, A.A. (2004) Accurate Surveying Measurements for Smart Structural Members. M.Sc. Thesis, Public Works Department, Faculty of Engineering, Mansoura University, El-Mansoura.

[2] Beshr, A.A. (2010) Development and Innovation of Technologies for Deformation Monitoring of Engineering Structures Using Highly Accurate Modern Surveying Techniques and Instruments. Ph.D. Thesis, Siberian State Academy of Geodesy, Novosibirsk, Surveying Techniques and Instruments.

[3] Daniele, I., *et al.* (1999) Long-Term Monitoring of a Concrete Bridge with 100+ Fiber Optic Long-Gage Sensors. *Proceedings of SPIE*, **3587**, 1-7.

[4] Erol, S. (2004) A General Review of the Deformation Monitoring Techniques and a Case Study: Analyzing Deformations Using GPS/Levelling. 1-7.

[5] Phares, B.M., *et al.* (2001) Reliability and Accuracy of Routine Inspection of Highway Bridges. *Journal of the Transportation Research Board*, **1749**, 81-92. https://doi.org/10.3141/1749-13

[6] Bennetts, *et al.* (2001) Using Data to Explore Trends in Bridge Performance. *Journal of Smart Infrastructure and Construction*, **171**, 14-28. https://doi.org/10.1680/jsmic.17.00022

[7] Handayani, *et al.* (2015) Preliminary Study of Bridge Deformation Monitoring Using GPS and CRP (Case Study: Suramadu Bridge). *Procedia Environmental Sciences*, **24**, 266-276. https://doi.org/10.1016/j.proenv.2015.03.035

[8] Mayunga, S.D. and Thabo, R. (2019) Deformation Monitoring of Lotsane Bridge Using Geodetic Method. *International Journal of Scientific Engineering and Research*, **7**, 21-27.

[9] Amin, N.M., *et al.* (2017) Condition Rating System of Bridges in Malaysia: A Case Study. *Journal of Engineering and Applied Sciences*, **12**, 787-791.

[10] Aktan, A.E., *et al.* (2020) Development of a Model Health Monitoring Guide for Major Bridges. Technical Report, Drexel University, Philadelphia.

[11] Meng, X., *et al.* (2011) Using Multi-Constellation GNSS and EGNOS for Bridge Deformation Monitoring. https://fig.net/resources/proceedings/2011/2011_lsgi/session_3a/meng_gogoi_dodson_roberts_brown.pdf

[12] Kessler, S.S. (2014) Spearing, Structural Health Monitoring of Composite Materials Using Piezoelectric Sensors. Department of Aeronautics and Astronautics, Massachusetts Institute of Technology, Cambridge.

[13] Amin, Z.M. and Akib, W.A.W. (2003) Experimental Detection of the Penang Bridge Vibration with Real Time Kinematic GPS. *International Symposium and Exhibition on Geoinformation*, Kuala Lumpur, 13-14 October 2003, 9.

[14] Park, H.S., Sohn, H.G., Kimi, I.S. and Park, J.H. (2008) Application of GPS to Monitoring of Wind Induced Responses of High-Rise Building. *The Structural Design of Tall and Special Buildings*, **17**, 117-132. https://doi.org/10.1002/tal.335

[15] Nehdi (2018) Condition Assessment of Reinforced Concrete Bridges: Current Practice and Research Challenges. *Infrastructures*, **3**, 36.

https://doi.org/10.3390/infrastructures3030036

[16] Featherstone, W.E., Denith, M.C. and Kirby, J.F. (1998) Strategies for the Accurate Determination of Orthometric Heights from GPS. *Survey Review*, **34**, 278-296. https://doi.org/10.1179/sre.1998.34.267.278

[17] Çelik, R.N., *et al.* (2001) Monitoring Deformation on Karasu Viaduct Using GPS and Precise Levelling Techniques. Kluwer Academic Publishers, Dordrecht. https://doi.org/10.1007/978-94-010-0696-5_28